*minerals*

MDPI

*Article*

# Evaluation of an Attachment–Detachment Kinetic Model for Flotation

**Mehdi Safari * and David Deglon**

Centre for Minerals Research, Department of Chemical Engineering, University of Cape Town, Private Bag Rondebosch, Cape Town 7700, South Africa; david.deglon@uct.ac.za

* Correspondence: Mehdi.Safari@uct.ac.za

Received: 28 September 2020; Accepted: 30 October 2020; Published: 2 November 2020


**Abstract:** This paper compares model predictions from a novel kinetic model with data from five fundamental single-mineral literature flotation datasets. The empirical correlations proposed by Safari and Deglon (2018) are modified to improve their robustness, requiring only a single best-fit regression coefficient per mineral type. Experimental and model-predicted rate constants were compared on a parity chart where a reasonable linear correlation was observed, with a gradient of 0.95 and an overall $R^2$ value of 0.97. Thereafter experimental and model-predicted trends from the flotation datasets were compared for particle size, contact angle, agitation, and gas flow rate. Model-predicted trends were reasonably accurate for most of the flotation datasets, but under-predicted the rate constant for larger particles for the data of Pyke (2004). In general model predictions were reasonably accurate, which is considered quite good, as these were obtained by fitting a single parameter per mineral type to several large flotation datasets, totaling 330 rate constants.

**Keywords:** flotation modelling; flotation kinetics

## 1. Introduction

Flotation is a common and widely used separation method for recovering minerals from ore bodies. For many years, researchers have been modelling flotation so as to improve plant performance [1–15]. There are several approaches to modelling flotation. Kinetic models are based on classical chemical reactor theory and are particularly useful for modelling flotation cells and circuits. However, most kinetic models are based on single rate constants, which accommodates the particle-bubble collision and attachment process, but does not allow for detachment. Deglon [16] developed a novel kinetic model that has both forward (collision/attachment) and reverse (detachment) rate constants. In a previous paper, Safari and Deglon [7] applied the kinetic model of Deglon [16] to the flotation data of Safari et al. [17] to generate a large dataset of attachment and detachment rate constants. This flotation dataset was obtained from 460 flotation tests for six mineral types (apatite, galena, hematite, pyrite, pentlandite, quartz). Empirical correlations for the attachment and detachment rate constants were developed using these data in terms of key flotation parameters. The attachment–detachment model and the associated empirical correlations were found to model the experimental data fairly well. The aim of this paper was to evaluate the efficacy of this model by comparing model predictions with experimental data from five fundamental single-mineral literature flotation datasets.

## 2. Methodology

### 2.1. Attachment–Detachment Kinetic Model

The attachment–detachment kinetic model for a laboratory batch flotation cell is shown in Equations (1) and (2), as presented by Safari and Deglon [7]. Equation (1) is a kinetic expression

defining the rate of change of the mass of particles in the pulp phase. The first term in the expression ($-k_aCV$) defines the rate at which particles are removed from the pulp due to collision/attachment. This is based on the assumption of first-order kinetics with respect to the particle volumetric concentration ($C$). Here, $k_a$ is the attachment rate constant, and $V$ is the volume of the flotation cell. The second term in the expression ($k_dC_sSV$) defines the rate at which particles return to the pulp phase from the gas phase due to detachment. This is also based on the assumption of first-order kinetics, but with respect to the particle surface concentration ($C_s$). Here, $k_d$ is the detachment rate constant, and $S$ is the specific bubble surface area.

Equation (2) is a kinetic expression defining the rate of change of the mass of particles on the gas phase, i.e., on bubble surfaces. The first two terms in this expression are identical to those in Equation (1) but of opposite sign, as they simply define the transfer of particles between the pulp and gas phases. The third term in the expression ($-S_bC_sA$) defines the rate at which particles leave the flotation cell as loaded bubbles are recovered as concentrate. Here, $S_b$ is the bubble surface area flux, and $A$ is the tank cross-sectional area. Equations (1) and (2) are solved simultaneously to determine recovery ($R$) in terms of $k_a$, $k_d$, flotation time ($t$), and the gas residence time in the flotation cell ($\tau_g$). The standard flotation rate constant ($k$) can be determined by fitting the expression $(1 - e^{-kt})$ to the recovery-time curve calculated using the model. The flotation rate constant may also be estimated using the expression $k = k_a/(1 + k_d\tau_g)$, as discussed by Safari and Deglon [7].

$$\frac{d(CV)}{dt} = -k_aCV + k_dC_sSV \quad (1)$$

$$\frac{d(C_sSV)}{dt} = k_aCV - k_dC_sSV - S_bC_sA \quad (2)$$

The empirical correlations for the attachment and detachment rate constants, and the associated exponents ($n$) obtained from Safari and Deglon [7], are given in Equations (3) and (4) and Table 1 respectively. Here $d_p$, $d_b$, $\rho$, $\theta$, and $\varepsilon$ refer to the particle size, bubble size, particle density, contact angle, and specific power input (or turbulent energy dissipation rate), respectively. The empirical exponents ($n_1$ to $n_5$) were observed to be fairly similar for the six mineral types (apatite, galena, hematite, pyrite, pentlandite, quartz) and over a broad range of particle size (1–650 μm), particle density (SG 3.2–7.6), bubble size (0.13–0.82 mm), contact angle (40–90°), and specific power input (0.1–5.0 W/kg). The exponents are empirical and only valid for this range of parameters, but are broadly consistent with findings from the flotation literature, as discussed by Safari and Deglon [7]. The equations are valid for the units specified in Table 1.

$$k_a = {d_p}^{n_1}(c_1 + c_2\varepsilon^{n_2})(1 - \cos\theta)^{n_3}{d_b}^{n_4}\rho^{n_5} \quad (3)$$

$$k_d = {d_p}^{n_1}(c_3 + c_4\varepsilon^{n_2})(1 - \cos\theta)^{n_3}{d_b}^{n_4}\rho^{n_5} \quad (4)$$

**Table 1.** Empirical coefficients and exponents for all minerals.

| Minerals | Attachment Rate Constant ($k_a$) | | Detachment Rate Constant ($k_d$) | |
|---|---|---|---|---|
| All Minerals | $n_1$ | 0.72 | $n_1$ | 2.17 |
| | $n_2$ | 0.91 | $n_2$ | 1.33 |
| | $n_3$ | 0.47 | $n_3$ | −1.17 |
| | $n_4$ | −0.77 | $n_4$ | 0.67 |
| | $n_5$ | 1.81 | $n_5$ | 0.67 |
| New Coefficients | $c_2$* | 1.17 | $c_4$* | $1.77 \times 10^{-5}$ |
| #Units: $d_p$ (μm), $d_b$ (mm), $\theta$ (°), $\rho$ (ton/m$^3$), $\varepsilon$ (W/kg) | | | | |

The coefficients ($c_1$ and $c_2$) for the attachment rate constant varied significantly between the mineral types and generally correlated with the natural floatability of the mineral. The coefficients ($c_3$ and $c_4$) for the detachment rate constant were similar for all minerals, but $c_3$ was typically an order of magnitude smaller than $c_4$. The constant coefficients ($c_2$* and $c_4$*) listed in Table 1 are used in this study and will be discussed further in Section 2.2.

### 2.2. Application of Attachment–Detachment Kinetic Model

Five fundamental single-mineral literature flotation datasets with a broad range of operating conditions were selected [18–22]. Deglon [18] conducted flotation tests on quartz in a 2.25 L batch stirred-tank flotation cell agitated by a Rushton turbine and a high speed spinning disc. Pyke [19] conducted flotation tests on quartz, chalcopyrite, and galena in a 2.25 L batch stirred-tank flotation cell agitated by a Rushton turbine. Newell [20] conducted flotation tests on quartz in a 2.25, 10, and 50 L batch stirred-tank flotation cell agitated by a Rushton turbine. Muganda et al. [21] conducted flotation tests on chalcopyrite in a 5 L bottom-driven laboratory batch flotation cell. Massey et al. [22] conducted flotation tests on quartz in a 10 L oscillating grid flotation cell.

Initially, the attachment–detachment kinetic model and the associated empirical correlations (Equations (3) and (4)) were applied to the five literature flotation datasets using the constant empirical exponents ($n_1$ to $n_5$) listed in Table 1. This is considered reasonable as they were found to be similar for six mineral types over a wide range of conditions. However, the four empirical coefficients ($c_1$, $c_2$, $c_3$, and $c_4$) were determined as individual best-fit regression values, as these depend on parameters such as mineral type and gas flow rate. The experimental and model-predicted rate constants were plotted on a parity chart, showing a reasonably good linear correlation with a gradient of 0.98 and an overall $R^2$ value of 0.97. However, the four best-fit regression coefficients ($c_1$, $c_2$, $c_3$, and $c_4$) were not sufficiently robust, as the five literature flotation datasets, although of good quality, were not as extensive as the data of Safari et al. [17] in terms of the large number of flotation tests (460), mineral types (6), and wide range of particle size, particle density, bubble size, contact angle, and power input. Here, various combinations of the four regression coefficients resulted in a similar goodness of fit.

Consequently, a number of simplifying assumptions and modifications were made in order to improve the robustness of the model by reducing the number of coefficients in Equations (3) and (4) before re-applying the attachment–detachment model to the five literature flotation datasets. The coefficients ($c_1$, $c_2$, $c_3$, and $c_4$) for the six mineral flotation datasets from the model of Safari and Deglon [7] were evaluated in terms of their relative magnitude and variability. For Equation (3), it was noted that although $c_1$ and $c_2$ varied significantly between the six mineral flotation datasets, the ratio of the two coefficients remained relatively constant. Hence, Equation (3) was rewritten in the form of Equation (5) by taking out $c_1$ as a common factor. This resulted in a new coefficient $c_2$* which is simply the ratio of $c_2$ to $c_1$ ($c_2$* = $c_2/c_1$). As discussed previously, for Equation (4), it was noted that $c_3$ and $c_4$ were similar in magnitude for the six mineral flotation datasets, but $c_3$ was an order of magnitude smaller than $c_4$. Hence, Equation (4) was rewritten as Equation (6), where $c_3$ is omitted as negligible, and $c_4$* is a new coefficient, which should remain similar in magnitude to $c_4$. The two new coefficients ($c_2$* and $c_4$*) in Equations (5) and (6) were expected to be similar for the six mineral flotation datasets for reasons discussed previously. Consequently, the attachment–detachment model and the revised empirical correlations for the rate constants (Equations (5) and (6)) were re-applied to the entire experimental flotation data of Safari et al. [17] in order to obtain common best-fit regression values for the two new constant coefficients ($c_2$* and $c_4$*), as shown in Table 1. This reduced the number of coefficients from four in Equations (3) and (4) to just one in Equations (5) and (6), i.e., $c_1$.

$$k_a = c_1(1 + c_2^*\varepsilon^{n_2})(1 - \cos\theta)^{n_3} {d_p}^{n_1} {d_b}^{n_4} \rho^{n_5} \quad (5)$$

$$k_d = c_4^*\varepsilon^{n_2}(1 - \cos\theta)^{n_3} {d_p}^{n_1} {d_b}^{n_4} \rho^{n_5} \quad (6)$$

The attachment–detachment model, used together with the revised empirical correlations for the rate constants (Equations (5) and (6)), the constant coefficients ($c_2$* and $c_4$*), and the exponents ($n_1$ to $n_5$) listed in Table 1, was applied to the five literature flotation datasets. Here, only the coefficient $c_1$ was determined as a best-fit regression value for each mineral type and/or gas flow rate, as this coefficient is considered to depend on these two parameters. The variables used for the determination of the kinetic constants from Equations (5) and (6) ($d_p$, $d_b$, $\theta$, $\rho$, $\varepsilon$) were obtained from the relevant literature. However, the gas residence time ($\tau_g$) could not be obtained for all conditions and had to be estimated from the bubble size and the associated bubble rise velocity.

## 3. Model Evaluation

### *3.1. Parity Chart*

Figure 1 compares the model-predicted and experimental flotation rate constants for the five literature flotation datasets with a single best-fit regression coefficient ($c_1$) for each dataset. Rate constants are plotted on a log scale, as they vary by orders of magnitude.

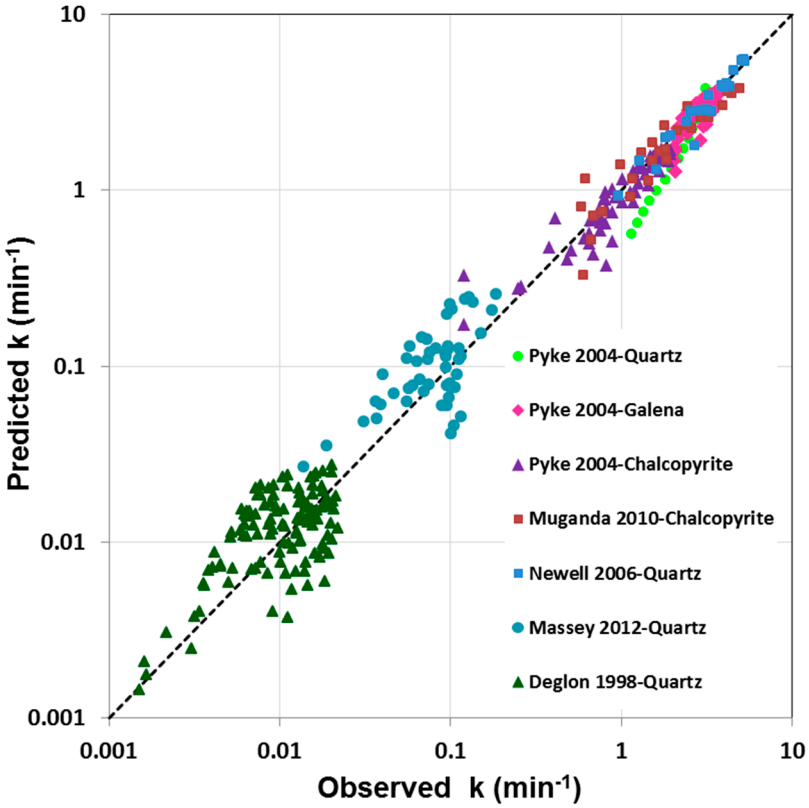


**Figure 1.** Model-predicted versus experimental flotation rate constant ($min^{-1}$).

Here, the seven individual test series shown for each mineral type cover a very broad range of operating conditions. There is a reasonable correlation between the experimental and model-predicted rate constants, yielding a linear correlation with a gradient of 0.95 and an overall $R^2$ value of 0.97. The parity chart does suggest that the model tends to under-predict the rate constant, as the gradient differs from unity, which will be discussed further in Section 3.3. However, in general, the parity chart suggests that the empirical coefficients and exponents in Table 1 are relatively robust, as these were determined by fitting a single parameter per mineral type to several large flotation datasets, totaling 330 rate constants and covering a wide range of mineral types, particle sizes, particle densities, bubble sizes, contact angles, and agitation/power inputs. Indeed, the authors are of the opinion that

the predictions are surprisingly good, given that the five researchers used very different operating conditions and that rate constants vary by several orders of magnitude.

### *3.2. Trend Prediction*

Figure 1 suggests that the attachment–detachment model, used together with the empirical correlations for the rate constants, models the literature flotation data relatively well. However, it is important that the model also predicts the trends in the experimental data. The following sections compare experimental versus model-predicted trends for particle size, contact angle, agitation, and gas flow rate. Here, a selection of trends from the literature flotation datasets is presented, showing both relatively good and poor model predictions.

#### 3.2.1. Particle Size

Figure 2 shows the relationship between the experimental and model-predicted flotation rate constants and the particle size for galena and chalcopyrite, from the literature flotation dataset of Pyke [19]. It is clear from this figure that the model predicts the trends in the experimental data for chalcopyrite reasonably well, but deviates from those for galena.

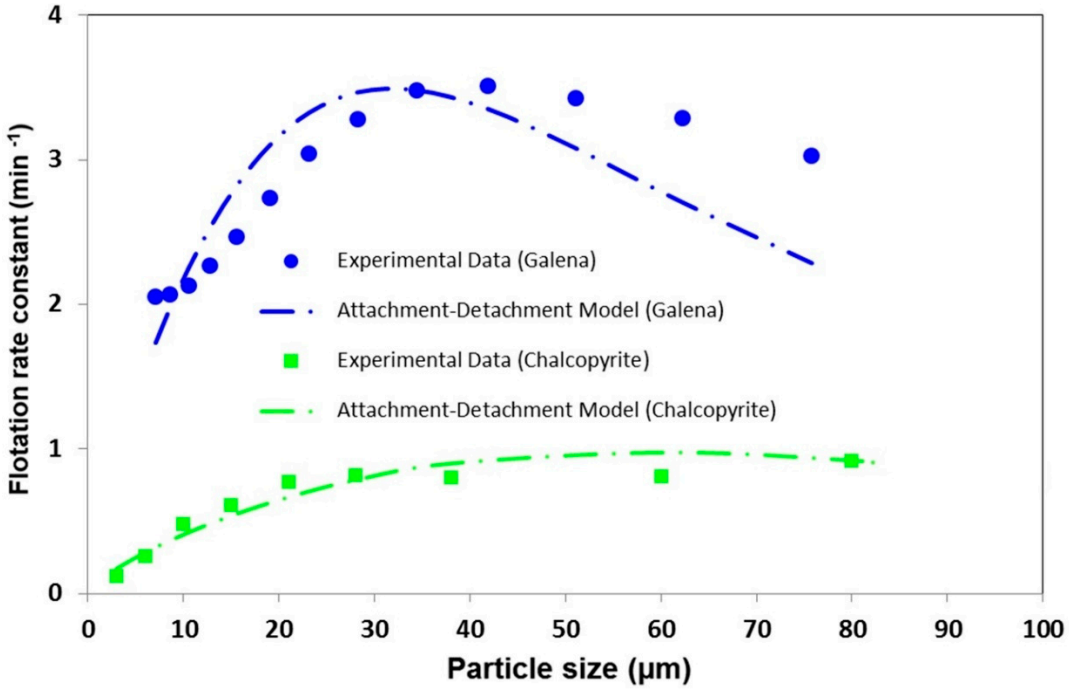


**Figure 2.** Comparison of experimental and model-predicted flotation rate constants as a function of particle size for chalcopyrite ($N$ = 720 rpm, $\theta$ = 62°) and galena ($N$ = 650 rpm, $\theta$ = 79°).

Here, the model is fairly accurate for the smaller particle sizes but significantly under-predicts the rate constant for larger particle sizes. This trend was found to occur predominantly in this flotation literature dataset and for the larger particle sizes, higher particle densities, lower contact angles, and higher impeller speeds. This suggest that the detachment rate constant calculated using Equation (6) is over-predicted under conditions where detachment rates, according to the presented model, are dominant. This may be due to issues with the model itself, the model being applied to a stirred/agitated system with associated large variations in turbulence ($\varepsilon$), the possibly over- restrictive requirement that the coefficient $c_4$* in the detachment expression is constant for all minerals/conditions, and/or sensitivities/issues related to the gas residence time. This will be discussed further in Section 3.3. It should however be noted that the under-prediction of the rate constant was observed predominantly in the flotation dataset of Pyke [19].

### 3.2.2. Contact Angle

Figure 3 shows the relationship between the experimental and model-predicted flotation rate constants and the particle size for chalcopyrite at three different contact angles, from the literature flotation dataset of Muganda et al. [21].

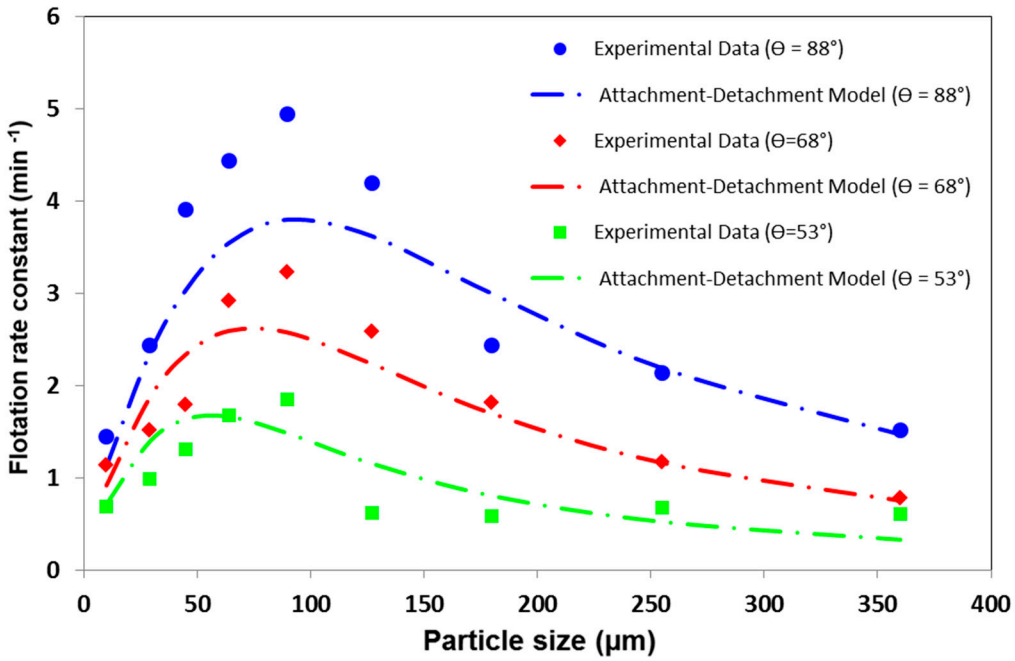


**Figure 3.** Comparison of experimental and model-predicted flotation rate constants as a function of particle size for chalcopyrite at three different contact angles ($N$ = 1200 rpm).

Here, the model gives a reasonable prediction of the trends in the experimental data for all three contact angles. There is a tendency for the model to under-predict the rate constants around the curve maxima, especially for the highest contact angle of $\theta$ = 88°. However, rate constants of above 3 to 5 min$^{-1}$ are simply considered "very high" and have no real implications for flotation modelling, as these particles are easily recovered. These model predictions are based on a single best-fit regression coefficient ($c_1$) and are considered quite good, given the broad range of contact angles ($\theta$ = 53° to 88°) and particle sizes ($d_p$ = 10 to 350 μm). It should be noted that the model-predicted flotation rate constants are accurate up to the large particle sizes (350 μm), and no under predication is observed, as found in the previous section.

### 3.2.3. Agitation/Power Input

Figures 4 and 5 show the relationship between the experimental and model-predicted flotation rate constants and the particle size for chalcopyrite and galena at two different impeller speeds, from the literature flotation dataset of Pyke [19].

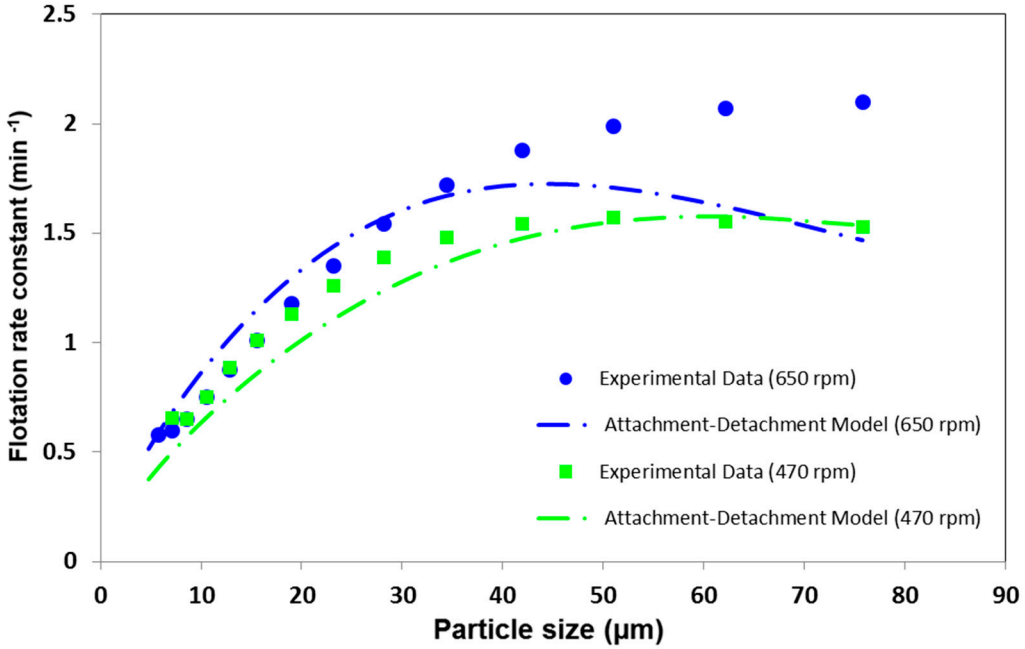


**Figure 4.** Comparison of experimental and model-predicted flotation rate constants as a function of particle size for chalcopyrite at two different impeller speeds ($\theta$ = 56°).

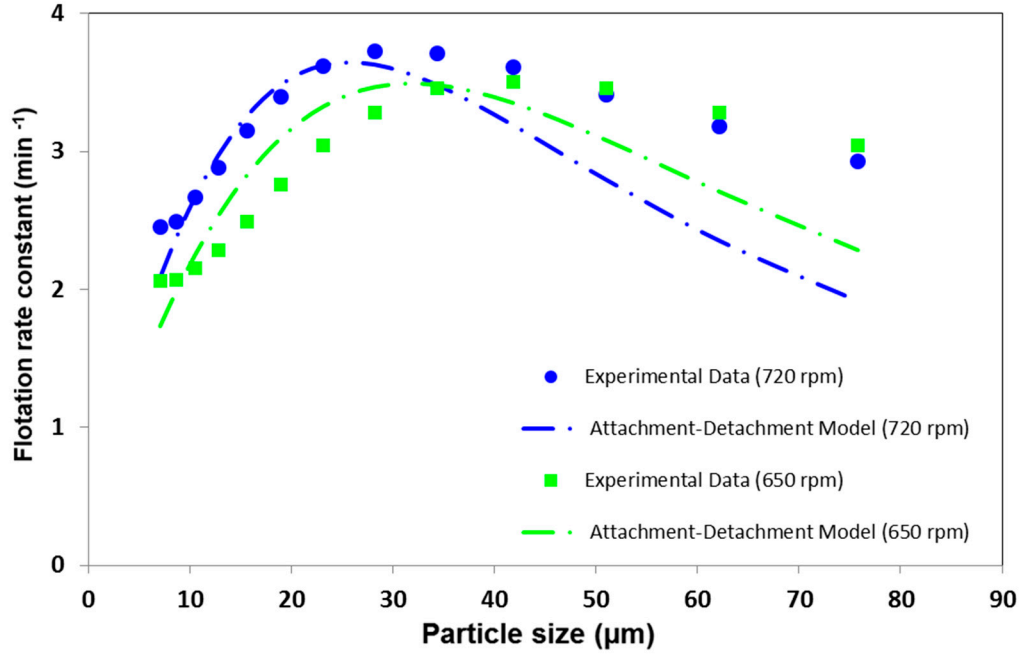


**Figure 5.** Comparison of experimental and model-predicted flotation rate constants as a function of particle size for galena at two different impeller speeds ($\theta$ = 79°).

Here, the model gives a reasonable prediction of the trends in the experimental data for chalcopyrite but at the lower impeller speed. The model also predicts the trends in the rate constants for the finer particles with moderate accuracy for all conditions, clearly showing the benefit of agitation on improving fine particle flotation [23–31]. However, the model significantly under-predicts the rate constant for larger particle sizes for both chalcopyrite at the higher impeller speed and galena at both impeller speeds. As noted in Section 3.2.1, this trend was found to occur predominantly in this flotation literature dataset and for the larger particle sizes, higher particle densities, lower contact angles, and higher power inputs. Here, the model under-predicts the rate constant for larger particle

sizes under conditions where, according to the presented model, detachment rates are dominant. This is clear from Figure 5, where the model-predicted rate constants are significantly worse for the higher impeller speed, where detachments effects are more pronounced. This will be discussed further in Section 3.3.

#### 3.2.4. Gas Flow Rate

Figure 6 shows the relationship between the experimental and model-predicted flotation rate constants and the particle size for quartz at three different gas flow rates, from the literature flotation dataset of Newell [20]. It is clear from this figure that the model predicts the trends in the experimental data reasonably well for all gas flow rates. The model-predicted flotation rate constants are also fairly accurate up to the larger particle sizes, with perhaps a slight tendency towards under-prediction for the largest particles. However, it should be noted that these model predictions are based on three best-fit regression coefficients ($c_1$), one for each gas flow rate. The coefficient $c_1$ accounts for the effect of both mineral type and gas flow rate, due to the attachment rate constant being defined as equivalent to the flotation rate constant. This means that model predictions should be more accurate, as there is an individual best-fit regression coefficient for each of the data series. However, this will have no effect on the tendency for the model to under-predict for larger particle sizes, as the detachment expression remains constant under all conditions, suggesting that the model is relatively accurate up to the larger particle sizes for this literature flotation dataset.

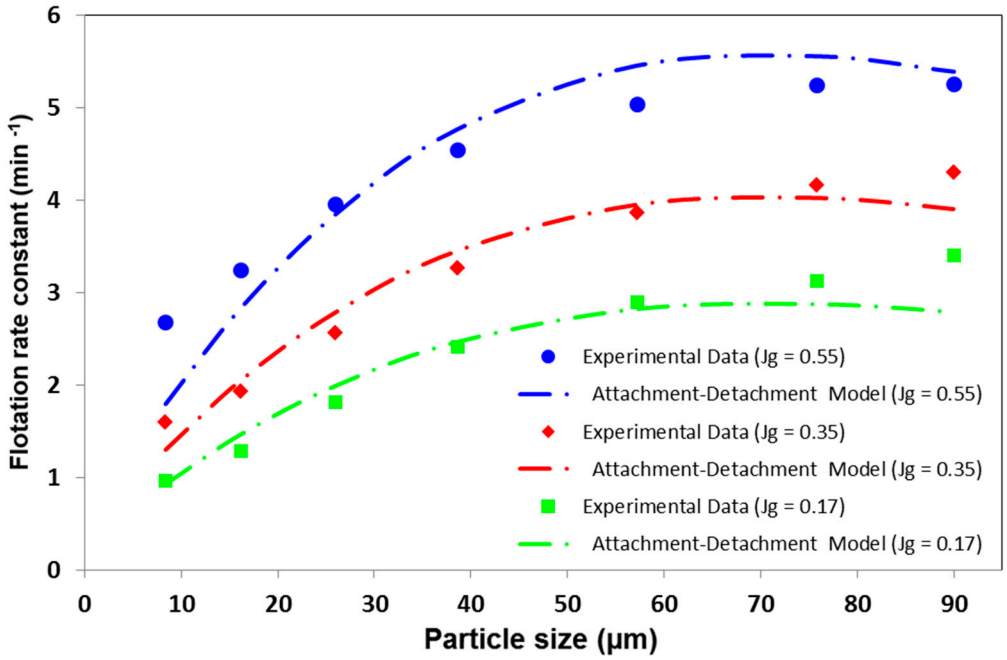


**Figure 6.** Comparison of experimental and model-predicted flotation rate constants as a function of particle size for quartz at three gas flow rates (superficial gas velocity $J_g$ in cm/s).

Perhaps of more significance is how the best-fit regression coefficients ($c_1$) vary with the gas flow rate. Gorain et al. [32] demonstrated that there is a linear correlation between the flotation rate constant and the bubble surface area flux ($6J_g/d_b$). The influence of the bubble size on the attachment rate constant is incorporated into Equation (5) as $1/{d_b}^{0.77}$. This is similar to the exponent of unity on the bubble size used in calculating the bubble surface area flux. Consequently, it is probable that the coefficients ($c_1$) will increase linearly with increasing superficial gas velocity, as the attachment rate constant was defined as equivalent to the flotation rate constant. These coefficients were found to be 0.015, 0.021, and 0.029 for the respective superficial gas velocities of 0.17, 0.35, and 0.55 cm/s. This yields a linear correlation between the coefficients and the superficial gas velocity, with a $R^2$ of

0.997. This is based on only three data points but was found to be applicable to the additional gas flow rates in the dataset of Newell [20], only three of which are shown in Figure 6 for illustrative purposes.

### *3.3. Evaluation*

The attachment–detachment model is considered useful for the modelling of flotation cells as it allows for both forward (collision/attachment) and reverse (detachment) kinetics, both of which occur in a flotation cell [16]. When applied to a batch flotation cell (Equations (1) and (2)), the model is complex to use, but it is far simpler when calculating the pulp-zone recovery ($R$) in a continuous mechanical flotation cell, as shown in Equation (7). Here, the pulp residence time ($\tau$) is calculated with the usual method from the volumetric flow rate of slurry and volume of pulp in the flotation cell ($V$). The gas residence time ($\tau_g$) is the residence time of bubble surface area in the flotation cell, but can be estimated by the gas residence time calculated on a volumetric basis using the gas flow rate ($Q$), the gas hold-up ($\Phi$), and the volume of pulp in the flotation cell by $\tau_g = (\Phi \cdot V)/Q$. Using this equation, and the equivalent expression for recovery calculated using the flotation rate constant, it is easy to demonstrate that the flotation rate constant ($k$) can be calculated from the attachment and detachment rate constants, as also shown in Equation (7).

$$R = \frac{k_a \tau}{1 + k_a \tau + k_d \tau_g} \qquad k = \frac{k_a}{1 + k_d \tau_g} \tag{7}$$

The attachment and detachment rate constants may be determined directly from Equation (7) and experimental data for mineral recovery. However, this may require an extensive dataset, as two best-fit regression rate constants need to be determined for each set of experimental conditions. Alternatively, the attachment and detachment rate constants may be estimated from the revised empirical correlations for the rate constants (Equations (5) and (6)), the constant coefficients ($c_2$* and $c_4$*), and the exponents ($n_1$ to $n_5$) listed in Table 1. These empirical correlations are a simplified and more robust version of the empirical correlations developed by Safari and Deglon [7], as applied to the extensive experimental flotation data of Safari et al. [17]. Here, only a single best-fit regression value is required for the coefficient ($c_1$) for each mineral type and/or gas flow rate. However, as the coefficient ($c_1$) is considered to vary linearly with the superficial gas velocity, only a single best-fit regression value is required for each mineral type at a known gas flow rate. The coefficient ($c_1$) may then be scaled linearly to other gas flow rates, relative to the known condition.

The attachment–detachment model is derived from the principles of classical chemical reactor theory, but the correlations for the rate constants and their associated coefficients and exponents are entirely empirical. Safari and Deglon [7] argue that the functional form of the correlations for the rate constants and the sign and magnitude of the exponents are to some extent consistent with theoretical and experimental findings from the flotation literature. However, the interpretation of the coefficients in the correlations is somewhat speculative. The coefficient $c_1$ is considered to depend on mineral type and gas flow rate, although as discussed previously, the influence of gas flow rate may be decoupled from this coefficient due to its linear dependence. The constant coefficients $c_2$* and $c_4$* are considered to determine the influence of agitation/power input on the attachment and detachment rate constants, as these coefficients are for terms containing the specific power input (or turbulent energy dissipation rate). The coefficient $c_2$* is quite large, suggesting that agitation/power input has a significant effect on increasing the rate of collision/attachment for all particles sizes. The coefficient $c_4$* is several orders of magnitude smaller, suggesting that detachment effects are minimal until particles are sufficiently large and/or power inputs are sufficiently high, as the detachment rate constant (Equation (6)) is dominated by the large exponents on these two values.

The attachment–detachment model, used together with the revised empirical correlations for the rate constants, gives a reasonable prediction of the trends in the experimental data of Safari et al. [17] and five additional literature flotation datasets. However, the model does under predict the rate constant in the literature flotation dataset of Pyke [19] under conditions where detachment rates,

according to the presented model, are dominant. This under-prediction results in a parity chart with a linear gradient of 0.95 rather than 1.0, as shown in Figure 1. This may be due to issues with the accuracy of the model itself or to a number of alternative reasons. Firstly, the empirical correlations for the rate constants were determined from an oscillating grid flotation cell, where turbulence ($\varepsilon$) is uniform throughout the vessel. Strictly speaking, when applying the model to an agitated flotation cell, one should either use volume-averaged rates determined for "zones" of similar turbulence or ideally use the model in a full CFD simulation (Computational Fluid Dynamics). Secondly, the coefficient ($c_4$* in the detachment expression was kept constant for all five literature flotation datasets, which is robust but may be excessively restrictive. The model makes a reasonably good prediction of all the trends in the literature flotation dataset of Pyke [19], when this coefficient is determined as a best-fit regression parameter. Thirdly, the detachment rate constant is dominated by the large exponents on the particle size and specific power input, which may influence the sensitivity of model predictions. Lastly, detachment rates are strongly dependent on both the detachment rate constant and the gas residence time.

The gas residence time used in the model predictions may have two significant issues, of which the less significant is that it was not measured in any of the literature flotation datasets and had to be estimated from the bubble size and associated bubble rise velocity. Of more significance is that the gas residence time used in the model predictions was that for the entire flotation cell. This is accurate for an oscillating grid flotation cell, where both agitation/turbulence ($\varepsilon$) and gas holdup ($\Phi$) are uniform throughout the vessel. However, in an agitated flotation cell, detachment rates are likely to dominate in the vicinity of the impeller zone, and the gas residence time in this region should be used. This will be considerably lower than that for the entire vessel, which may result in lower predicted detachment rates if the detachment rate constant in this region is not sufficiently large. Here, model predictions may be more accurate when using the "multi-zone" or CFD approach discussed previously, with rate constants and residence times determined for each "zone" or node in the flotation cell. It should however be noted that the under-prediction of the rate constant was predominantly observed in the flotation dataset of Pyke [19] and not in the other four datasets.

## 4. Conclusions

This paper compared model predictions from an attachment–detachment kinetic model, and associated empirical correlations for the rate constants, with experimental data from five fundamental single-mineral literature flotation datasets. Initially, the empirical correlations proposed by Safari and Deglon [7] were modified to improve their robustness, requiring only a single best-fit regression coefficient ($c_1$) for each mineral type. Experimental and model-predicted rate constants were compared on a parity chart, where a reasonable linear correlation was observed, with a gradient of 0.95 and a $R^2$ value of 0.97. Thereafter, experimental and model-predicted trends from the literature flotation datasets were compared for particle size, contact angle, agitation, and gas flow rate. Model-predicted trends were reasonably accurate for most of the literature flotation datasets. However, the model significantly under-predicted the rate constant for the larger particle sizes for the data of Pyke [19], particularly for higher particle densities, lower contact angles, and higher impeller speeds. This was attributed to a number of potential issues, including the large variations in turbulence in stirred cells, the use of a constant detachment expression for all minerals, and sensitivities/issues related to the gas residence time. Model predictions may be more accurate when using a "multi-zone" or CFD approach to modelling flotation cells. However, in general, model predictions were found to be reasonably accurate, which is considered quite good, given that these were obtained by fitting a single parameter per mineral type to several large flotation datasets, totaling 330 rate constants and covering a wide range of mineral type, particle size, particle density, bubble size, contact angle, and agitation/power input.

**Author Contributions:** Conceptualization, M.S. and D.D.; methodology, M.S.; software, M.S.; validation, M.S.; formal analysis, M.S.; investigation, M.S. and D.D.; writing—original draft preparation, M.S.; writing—review and editing, M.S. and D.D. All authors have read and agreed to the published version of the manuscript.

**Funding:** This research received no external funding.

**Conflicts of Interest:** The authors declare they have no conflict of interest.

## References

1. Gaudin, A.M. *Flotation*, 2nd ed.; McGraw-Hill: New York, NY, USA, 1957.
2. Bascur, O.A.; Herbst, J.A. Dynamic Modeling of a Flotation Cell with a View toward Automatic Control. *CIM Bull.* **1982**, *75*, 111–122.
3. Deng, H.; Mehta, R.K.; Warren, G.W. Numerical modeling of flows in flotation columns. *Int. J. Miner. Process.* **1996**, *48*, 61–72. [CrossRef]
4. Pyke, B.L.; Duan, J.; Fornasiero, D.; Ralston, J. From turbulence and collision to attachment and detachment: A general flotation model. In *Flotation and Flocculation from Fundamentals to Applications*; International Workshop on Flotation and Flocculation: Kailua-Kona, HI, USA, 2002; pp. 77–89.
5. Pyke, B.; Fornasiero, D.; Ralston, J. Bubble particle heterocoagulation under turbulent conditions. *J. Colloid Interface Sci.* **2003**, *265*, 141–151. [CrossRef]
6. Bloom, F.; Heindel, T.J. Modelling flotation separation in a semi-batch Processing. *Chem. Eng. Sci.* **2003**, *58*, 353–365. [CrossRef]
7. Safari, M.; Deglon, D. An Attachment-Detachment Kinetic Model for the Effect of Energy Input on Flotation. *Miner. Eng.* **2018**, *117*, 8–13. [CrossRef]
8. Dobby, G.S.; Savassi, O.N. An Advanced Modelling Technique for Scale-Up of Batch Flotation Results to Plant Metallurgical Performance. In *Centenary of Flotation Symposium*; AusIMM: Melbourne, Australia, 2005.
9. Sherrell, I.; Yoon, R.H. Development of a turbulent flotation model. In *Centenary of Flotation Symposium*; AusIMM: Melbourne, Australia, 2005.
10. Barnwal, J.P.; Majumder, A.K.; Govindarajan, B.; Rao, T. Modeling of coal flotation in a batch and continuous cell operation, Part 1-kinetic approach. *Coal Prep.* **2006**, *26*, 123–136. [CrossRef]
11. Koh, P.; Smith, L. Experimental validation of a flotation cell model. In Proceedings of the 25th International Mineral Processing Congress (IMPC 2010), Brisbane, Australia, 6–10 September 2010.
12. Goel, S.; Jameson, G.J. Detachment of particles from bubbles in an agitated vessel. *Miner. Eng.* **2012**, *36–38*, 324–330. [CrossRef]
13. Karimi, M.; Akdogan, G.; Bradshaw, S.M. A computational fluid dynamics model for the flotation rate constant, Part II: Model validation. *Miner. Eng.* **2014**, *69*, 214–222. [CrossRef]
14. Hoseinian, F.S.; Rezai, B.; Kowsari, E.; Safari, M. A hybrid neural network/genetic algorithm to predict Zn(II) removal by ion flotation. *Sep. Sci. Technol.* **2020**, *55*, 1197–1206. [CrossRef]
15. Hoseinian, F.S.; Rezai, B.; Safari, M. A new kinetic model for zinc ion removal from synthetic wastewater. In Proceedings of the 10th European Metallurgical Conference (EMC 2019), Düsseldorf, Germany, 23–26 June 2019; pp. 1409–1416.
16. Deglon, D. A novel attachment—detachment kinetic model. In *Flotation and Flocculation—From Fundamentals to Applications*; International Workshop on Flotation and Flocculation: Kailua-Kona, HI, USA, 2002; pp. 109–116.
17. Safari, M.; Harris, M.C.; Deglon, D.A.; Filho, L.L.; Testa, F. The effect of energy input on flotation kinetics. *Int. J. Miner. Process.* **2016**, *156*, 108–115. [CrossRef]
18. Deglon, D.A. A Hydrodynamic Investigation of Fine Particle Flotation in a Batch Flotation Cell. Ph.D. Thesis, Department of Chemical Engineering, University of Cape Town, Cape Town, South Africa, 1998.
19. Pyke, B. Bubble–Particle Capture in Turbulent Flotation Systems. Ph.D. Thesis, Ian Wark Research Institute, University of South Australia, Mawson Lakes, Australia, 2004.
20. Newell, R. Hydrodynamics and Scale-Up in Rushton Turbine Flotation Cells. Ph.D. Thesis, Ian Wark Research Institute, University of South Australia, Mawson Lakes, Australia, 2006.
21. Muganda, S.; Zanin, M.; Grano, S.R. Influence of particle size and contact angle on the flotation of chalcopyrite in a laboratory batch flotation cell. *Int. J. Miner. Process.* **2011**, *98*, 150–162. [CrossRef]
22. Massey, W.T.; Harris, M.C.; Deglon, D.A. The effect of energy input on the flotation of quartz in an oscillating grid flotation cell. *Miner. Eng.* **2012**, *36–38*, 145–151. [CrossRef]

23. Safari, M.; Hoseinian, F.S.; Deglon, D.; Filho, K.L.L.; Souza, T. Investigation of the reverse flotation of iron ore in three different flotation cells: Mechanical, oscillating grid and pneumatic. *Miner. Eng.* **2020**, *150*, 106283. [CrossRef]
24. Tabosa, E. The Effect of Cell Hydrodynamics on Flotation Kinetics. Ph.D. Thesis, University of Queensland, Brisbane, Australia, 2012.
25. Hoseinian, F.S.; Rezai, B.; Safari, M.; DADeglon Kowsari, E. Effect of hydrodynamic parameters on nickel removal rate from wastewater by ion flotation. *J. Environ. Manag.* **2019**, *244*, 408–414. [CrossRef] [PubMed]
26. Safari, M.; Harris, M.; Deglon, D. The effect of energy input on the flotation of a platinum ore in a pilot-scale oscillating grid flotation cell. *Miner. Eng.* **2017**, *110*, 69–74. [CrossRef]
27. Tabosa, E.; Runge, K.; Holtham, P.; Duffy, K. Improving flotation energy efficiency by optimizing cell hydrodynamics. *Miner. Eng.* **2016**, *96–97*, 194–202. [CrossRef]
28. Hoseinian, F.S.; Rezai, B.; Kowsari, E.; Safari, M. Effect of impeller speed on the Ni(II) ion flotation. *Geosyst. Eng.* **2018**, *22*, 161–168. [CrossRef]
29. Safari, M.; Harris, M.; Deglon, D. The effect of energy input on the flotation kinetics of galena in an oscillating grid flotation cell. In Proceedings of the 27th International Mineral Processing Congress (IMPC 2014), Santiago, Chile, 20–24 October 2014.
30. Testa, F.; Safari, M.; Deglon, D.; Filho, L.L. Influence of agitation intensity on flotation rate of apatite particles. *Rev. Esc. Minas* **2017**, *70*, 491–495. [CrossRef]
31. Safari, M.; Hoseinian, F.S.; Deglon, D.; Filho, K.L.L.; Souza, T. Investigation of the reverse flotation of hematite in three different types of laboratory flotation cells. In Proceedings of the 29th International Mineral Processing Congress (IMPC 2018), Moscow, Russia, 17–21 September 2018; pp. 1376–1383.
32. Gorain, B.K.; Franzidis, J.P.; Manlapig, E.V. Studies on impeller type, impeller speed and air flow rate in an industrial scale flotation cell. Part 4: Effect of bubble surface area flux on flotation kinetics. *Miner. Eng.* **1997**, *10*, 367–379. [CrossRef]


**Publisher's Note:** MDPI stays neutral with regard to jurisdictional claims in published maps and institutional affiliations.

© 2020 by the authors. Licensee MDPI, Basel, Switzerland. This article is an open access article distributed under the terms and conditions of the Creative Commons Attribution (CC BY) license (http://creativecommons.org/licenses/by/4.0/).